A Physical Model Reveals the Mechanochemistry Responsible for Dynein's Processive Motion

Denis Tsygankov,[†] Adrian W. R. Serohijos,[§] Nikolay V. Dokholyan,[‡] and Timothy C. Elston[†*]
[†]Department of Pharmacology and [‡]Department of Biochemistry and Biophysics, The University of North Carolina at Chapel Hill, Chapel Hill, North Carolina; and [§]Department of Chemistry and Chemical Biology, Harvard University, Cambridge, Massachusetts

ABSTRACT The molecular motor dynein is associated with various cellular activities, such as directed transport along microtubules and the rhythmic beating of the axoneme. Because of the size and complexity of the protein, a detailed understanding of the mechanochemistry that drives dynein's processive motion is lacking. To overcome this deficiency, we developed the first (to our knowledge) computational model for two-headed dynein that couples conformational changes of the motor's subunits to the biochemical steps involved in ATP hydrolysis. Analysis of the model provides what we believe are several novel insights into how the protein functions: 1), structural constraints limit the motion of the free microtubule binding domain to one dimension, increasing the efficiency with which this domain finds a binding site; 2), in addition to the power stroke of the bound head, recovery of the free head to a pre-power-stroke conformation is required for this head to reach a forward binding site; 3), the order in which the power stroke and recovery transitions occur affects the probability of back-stepping; and 4), the existence of multiple equilibria in the motor's bending energy provides a mechanism for processive back-stepping. To the best of our knowledge, our computational model provides the first complete mechanochemical description of the motor protein dynein, and the findings presented here should motivate new experimental investigations to test its predictions.

INTRODUCTION

The protein dynein is a molecular motor that is involved in intracellular trafficking and force generation (1–3). In particular, cytoplasmic dynein transports various types of cargo, including vesicles and organelles, toward the cell nucleus by walking along microtubules (4). Each dynein monomer or head is a motor unit that is capable of using the free energy of ATP hydrolysis to generate force (5). However, a homodimer of two heads is required to ensure that the motor maintains contact with the microtubule during processive stepping.

The mechanisms used by dynein to generate force and directed movement remain unclear (6–8). To efficiently couple the free energy of ATP hydrolysis to force generation, the individual dynein heads must synchronize their hydrolysis cycle (ATP binding, hydrolysis, and release of ADP and Pi) with two mechanical cycles: 1), attachment to and detachment from the microtubule; and 2), transitions between the conformational states of the molecule (9,10). Additionally, for processive stepping to occur, the mechanochemical cycles of the two heads must be coordinated and occur out of phase (11–13).

Various mechanisms for energy transduction by dynein have been proposed. A common model is one in which the stalk (the subunit that extends from the motor domain and interacts with the microtubule) acts as a lever arm that adopts two distinct conformations with respect to the microtubule (6,14). The transition between the two conformations generates a power stroke that moves the motor forward. Alternatively, it has been suggested (7) that the orientation of the stalk remains fixed, and movement of the tail linker (the subunit that connects the tail domain with the motor domain) is responsible for force generation. A third model (8) proposes a cyclic extension and retraction of the tail, with the stalk acting as a grappling hook that catches and holds the microtubule as the tail retracts. Unfortunately, all of these models have only been described qualitatively and do not consider any potential cooperative motion of the two heads. Here we present a mechanochemical model of dimeric dynein that couples the known biochemistry for monomeric dynein to the experimentally determined conformational changes in the head subunits induced by changes in the biochemical state of the motor. Computer simulations of the model provide a detailed explanation for how this complex protein efficiently moves along microtubules, and lead to a number of experimentally testable predictions.

RESULTS AND DISCUSSION

Coarse-grained structural model of homodimeric dynein

Using electron microscopy (EM), Burgess et al. (14) imaged individual dynein heads and identified structural states corresponding to pre- and post-power-stroke conformations. The ensemble of EM images generated by Burgess et al. not only characterized the equilibrium (mean) shape of the head in each conformational state but also provided distributions for the relative positions of the stalk and tail subunits (Fig. 1, *A* and *B*). Our analysis of the EM images revealed that the structure of each head can be defined by three

Submitted March 18, 2011, and accepted for publication May 18, 2011.

*Correspondence: telston@med.unc.edu

Editor: Claudia Veigel.

0006-3495/11/07/0144/7 $2.00

doi: 10.1016/j.bpj.2011.05.043

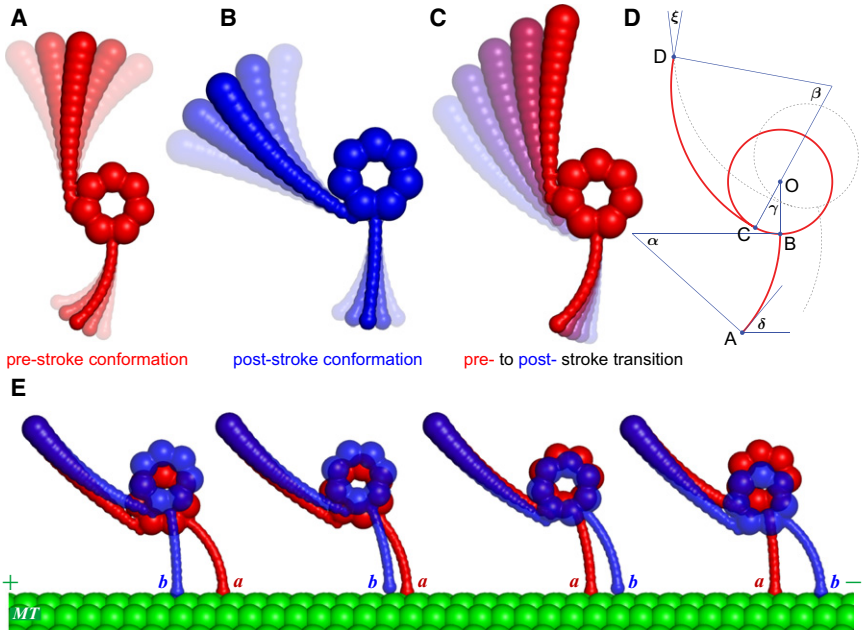

FIGURE 1 Structural model of dynein. (*A*) The average pre-power-stroke conformation plus 3 SDs in the positions of the tail and stalk. (*B*) The post- power-stroke conformation plus 3 SDs in the position of the tail and the stalk. (*C*) The change in geometry as the head transitions from a pre- to post-power-stroke conformation (*red* to *blue* in color, *black* to *gray* in black and white). In *A–C* the position of the AAA^+ ring is fixed in space. (*D*) A schematic diagram of dynein showing the five angles used to describe its shape. The angles α and β parameterize the curvature of the stalk and the tail, respectively. The angle γ (BOC) assumes two distinct values that correspond to pre- and post-power-stroke conformations. The angles ξ and δ characterize relative orientation of the heads at the point of the tail junction and microtubule attachments, respectively. (*E*) Representative snapshots showing the relative positions of the heads during a forward step. The bound head (*a*) remains attached to the microtubule (MT) while undergoing the power stroke. The free head (*b*) moves from a trailing to leading position while undergoing the recovery stroke (see also Fig. S1, Table S1, and Movie S1).

degrees of freedom: angles α and β , which characterize the curvature of the stalk and tail, respectively, and angle γ, which describes the relative position of the stalk and tail (Fig. 1 *D*). By the term "tail", we mean the portion of the N sequence that lies upstream of the N-terminus of the linker, which spans the AAA^+ ring, up to the point at which the heads are connected. In a previous study (15) we used experimental images to estimate the distribution for these angles and derive the bending free energy for the head in both pre- and post-power-stroke conformations (Fig. 1, *A–C*, and Fig. S1 in the Supporting Material). This analysis established that the minimum energy conformation of dimeric dynein when both heads are bound to the microtubule is achieved when the two stalks are attached to binding sites 8.2 nm apart with the front and rear heads in pre- and post-power-stroke conformations, respectively (11,15) (Supporting Material).

To gain insight into the motion of the motor during its step cycle, we started the dimer from the minimum energy conformation described above and continuously transformed the front (back) head from the pre- (post-) power-stroke conformation to the post- (pre-) power-stroke conformation. The microtubule binding domain (MTBD) of the front head was held fixed and the MTBD of the rear head was free to move. Fig. 1 *E* shows snapshots of the resulting motion (Movie S1). The free head's MTBD remains in close proximity to the microtubule until it reaches the binding site immediately in front of the bound head. This behavior highlights a central result of the mechanochemical model presented in the following sections. Dynein's structure constrains the motion of MTBD of the free head to one dimension, thereby increasing the efficiency with which the free head finds the appropriate binding site.

Stochastic model for the dynamics of the homodimer

Motivated by our ability to extract accurate low-dimensional representations of the conformational states of dynein's subunits from experimental data, we developed a computational model for the stochastic dynamics of a dynein homodimer. The model is based on the angles defined in Fig. 1 *D* and the bending energies derived from the observed fluctuations in these angles. Additional degrees of freedom taken into account in the model are the angles formed by the tail subunits, ξ, and the stalk and microtubule, δ. The dynamics of each angle is modeled with the use of a Langevin equation (Supporting Material).

We first used the stochastic model to investigate how efficiently the free head finds the appropriate microtubule-binding site. One feature that distinguishes dynein from other linear motors, such as conventional kinesin or myosin V, is its large size. The entire dynein molecule is up to ~80 nm long, with each head weighing ~0.5 MDa (compared with kinesin's motor domain of ~40 kDa). Given this large size and the relatively wide range of motion of the stalk and tail (Fig. 1, *A–C*), it is reasonable to expect that the MTBD explores a large volume of space and frequently encounters binding sites to the rear of the attached head. Therefore, our first goal was to use the model to investigate how the motor overcomes these potential impediments to forward progress. Stochastic simulations were run with the bound head in the post-power-stroke conformation and the free head in the pre-power-stroke conformation, the presumptive state of the motor when reattachment occurs. Surprisingly, the simulations reveal that when the motor is in this state, the motion of the MTBD of the free head is constrained to

a region near the microtubule-binding site directly in front of the attached head (Fig. 2 *A*). Although the stalk tip can fluctuate to >30 nm above the microtubule, its motion along the microtubule remains within a region of <8 nm width centered on the binding site. Furthermore, because the motion of the stalk is occluded by the microtubule, the MTBD encounters the binding site with high frequency.

To investigate whether this property depends sensitively on the angle between the stalk and microtubule (δ), we increased the rotational flexibility of this angle so that its standard deviation (SD) increased from 1.5° to 15° about the mean of 90°. Although this change did broaden the distribution of the MTBD (Fig. 2 *B*), it produced only a modest increase in the frequency with which the MTBD reached the binding site 16.4 nm in front of the bound head. Similarly, increasing the flexibility of the angle between the two tails (ξ), assumed to have a mean 0°, did not significantly affect the distribution for the MTBD

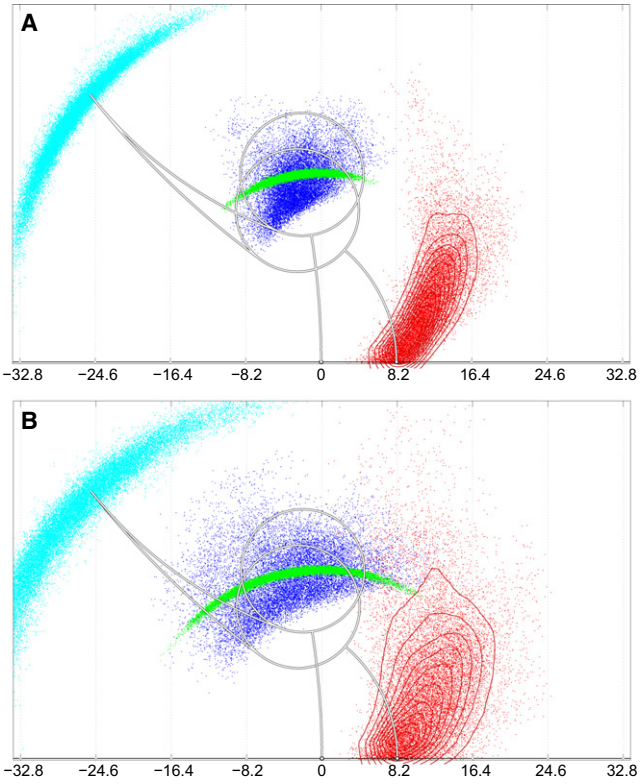

FIGURE 2 Range of motion for the two heads. Simulation results for the dynamics of dynein when the bound head is in the post-power-stroke conformation and the free head is in the pre-power-stroke conformation. Red dots are the distribution of positions for the free head's MTBD. The red lines are contours of equal probability. Green and blue dots are the distributions for the positions of the ring centers of the bound and unbound head, respectively. Cyan dots are the distribution of positions for the point where the two tails connect. The conformation with both heads bound to the microtubule has been drawn for reference. (*A*) Tight binding: In this panel, the angle formed by the bound head and microtubule has a Gaussian distribution centered around perpendicular and 3 SDs of 5°. (*B*) Flexible binding: The same as *A* except with a 3 SD range of 45° (see also Fig. S2).

(Supporting Material). Thus, our results demonstrate that the equilibrium structure of dimeric dynein constrains the motion of the free head so that its MTBD is closely positioned near the appropriate binding site (see also Fig. S2). We note that there are other potential sources of structural flexibility that also might contribute to dynein's range of motion. For example, Roberts et al. (16) demonstrated that the stalk undergoes a small nucleotide-dependent tilt relative to the AAA^+ ring. Similarly, the N-terminus of the linker, which we assume remains at the edge of AAA^+ ring (17), may deviate radially outward during the power stroke. A more-detailed structural model is needed to account for these effects. However, we do not believe they would contribute significantly to dynein's flexibility.

Comparison with the step-size distribution

Although experimental studies suggest that cytoplasmic dynein takes predominantly 8.2 nm steps, steps of up to 24.6 nm and back-steps of up 16.4 nm are also observed (18). To investigate which properties of the motor contribute to the additional variability in the experimentally measured step-size distribution, we perform simulations as follows: Each simulation starts with detachment of the rear head from the microtubule in the post-power-stroke conformation, and the front head bound in the pre-power-stroke configuration. The subsequent power stroke of the bound head and recovery of the free head are simulated as independent stochastic transitions in the coordinate γ for each head (Fig. 1 *D*). To model the two conformational states, the free energy for each γ is assumed to have the form of a double-well potential (Supporting Material). The shape of the potential is adjusted to produce a stepping rate consistent with experimentally observed rate of ~100 steps per second. During a conformational transformation, the equilibrium positions and stiffnesses of angles α and β are updated to take on the values derived from the EM images for the current state (see Appendix, Supporting Material, and Table S1). The conformational transitions of the two heads bias the movement of the free head so that the MTBD tends to be positioned near the appropriate binding site (Fig. 1 *E* and Fig. S3 *A*). However, any time the MTBD comes within a distance of 0.2 nm to a binding site, it is assumed to attach to the microtubule and the step size is recorded.

The results for the computed step-size distributions and a comparison with the experimental results of Reck-Peterson et al. (18) are presented in Fig. 3 *A*. Note that it was not experimentally possible to detect cases in which the free head reattached to the site from which it was originally bound (i.e., a step size of 0). This limitation accounts for the discrepancy between the experimental data and the model for step sizes of 0. We include such steps in the modeling results because they reveal that the frequency of futile cycles increases when the flexibility in the angle (δ), describing the orientation of the stalk relative to the microtubule

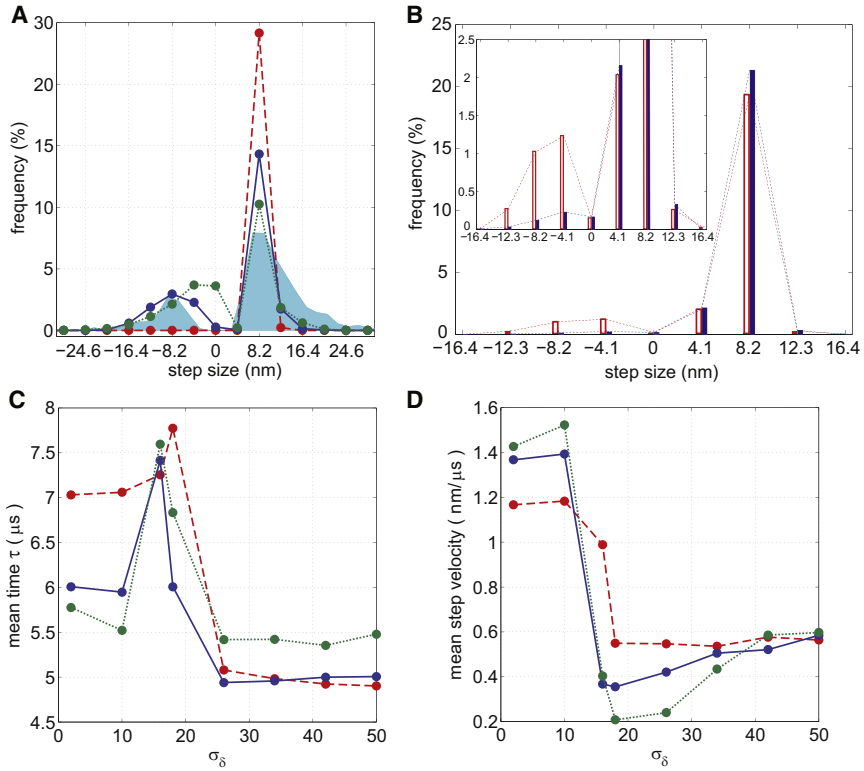

FIGURE 3 Stepping characteristics. (*A*) Comparison of experimental (*shaded area*) and simulated (*lines*) step-size distributions for the motor's center of mass. The experimental results are taken from Reck-Peterson et al. (18). The different line styles correspond to different rotational flexibilities in the angles δ and ξ that describe the attachment of the MTBD to the microtubule and the connection of the two tails, respectively. The distributions for these angles are characterized by their SDs; σ_δ and σ_ξ: (*dashed line*) [σ_δ, σ_ξ] = [2°, 40°]; (*solid line*) [16°, 40°]; (*dotted line*) [34°, 21°]. (*B*) Step-size distribution when the recovery of the unbound head precedes the power stroke of the bound head (*open histogram*) and vice versa (*solid histogram*; see also Fig. S3). (*C*) Mean time τ for the free head to find a binding site as function of σ_δ, for σ_ξ = 2° (*dashed line*), 21° (*solid line*), and 40° (*dotted line*). (*D*) Mean step velocity $<L>/\tau$, where $<L>$ is the average step size, as a function of σ_δ, for σ_ξ = 2° (*dashed line*), 21° (*solid line*), and 40° (*dotted line*).

orientation, increases. The figure shows results for three different combinations of stiffness in the angles between the stalk and microtubule (δ), and between the tails ξ. The simulated distribution in which the SDs in the angles δ and ξ are 16° and 40°, respectively, is in close agreement with the experimental results. Thus, the model predicts that considerable flexibility in the angles δ and ξ is required to achieve step sizes of >8.2 nm and back-stepping.

Although these simulations accurately reproduce the distribution of back-steps and correctly capture the predominance of 8.2 nm steps, the model underestimates the frequency of the large (>8.2 nm) forward steps measured by Reck-Peterson et al. (18). However, our results are consistent with the step-size distributions reported by Toba et al. (19), who did not observe steps larger than 16 nm. A possible explanation for this discrepancy in the step-size distribution is that the form of dynein studied by Reck-Peterson et al. (18) occasionally assumes a less compact conformation in which one or both tail linkers are undocked from the AAA^+ rings. Indeed, Carter et al. (17) recently showed that the construct used by Reck-Peterson et al. (18), in which truncated dynein heads were dimerized by glutathione S-transferase (GST), has a pseudo-twofold symmetry with the AAA^+ rings apposing each other and the stalks pointing in opposite directions. With this construct, it is presumed that for both heads to bind to the microtubule, one of the linkers must detach from the head. This suggests that linker undocking might increase dynein's flexibility and its ability to take forward steps of >16 nm.

Next we investigated how the order of the power stroke and recovery affects the step-size distribution (Fig. 3 *B*). We ran two types of simulations: one in which the power stroke of the bound head is not initiated until the recovery of the free head is completed (*open histogram*), and one in which recovery does not occur until completion of the power stroke (*solid histogram*). Our results show that back-stepping is less prevalent when the power stroke precedes recovery. This result has a structural explanation. The pre-power-stroke conformation of the dynein monomer is more elongated than the post-power-stroke conformation (compare Fig. 1, *A* and *B*). During the power stroke, the bound head shortens and effectively pulls the diffusing head in the forward direction. If the free head has already undergone the recovery transition, it assumes the elongated conformation and its motion is obstructed by the microtubule during the power stroke (Fig. S3, *B* and *C*). This barrier to diffusion makes it more likely that the free head will encounter a site behind the attached head (Fig. 4 *D*). These results suggest that a coupling mechanism between the heads may exist to ensure that the attached head will undergo the power stroke before the recovery transition of the free head is completed.

Calculation of the mean search time and step velocity

We next investigated how flexibility in the angles δ and ξ affects the time required for the free head to find a binding site (Fig. 3 *C*). Initially, as the flexibility of the stalk-microtubule

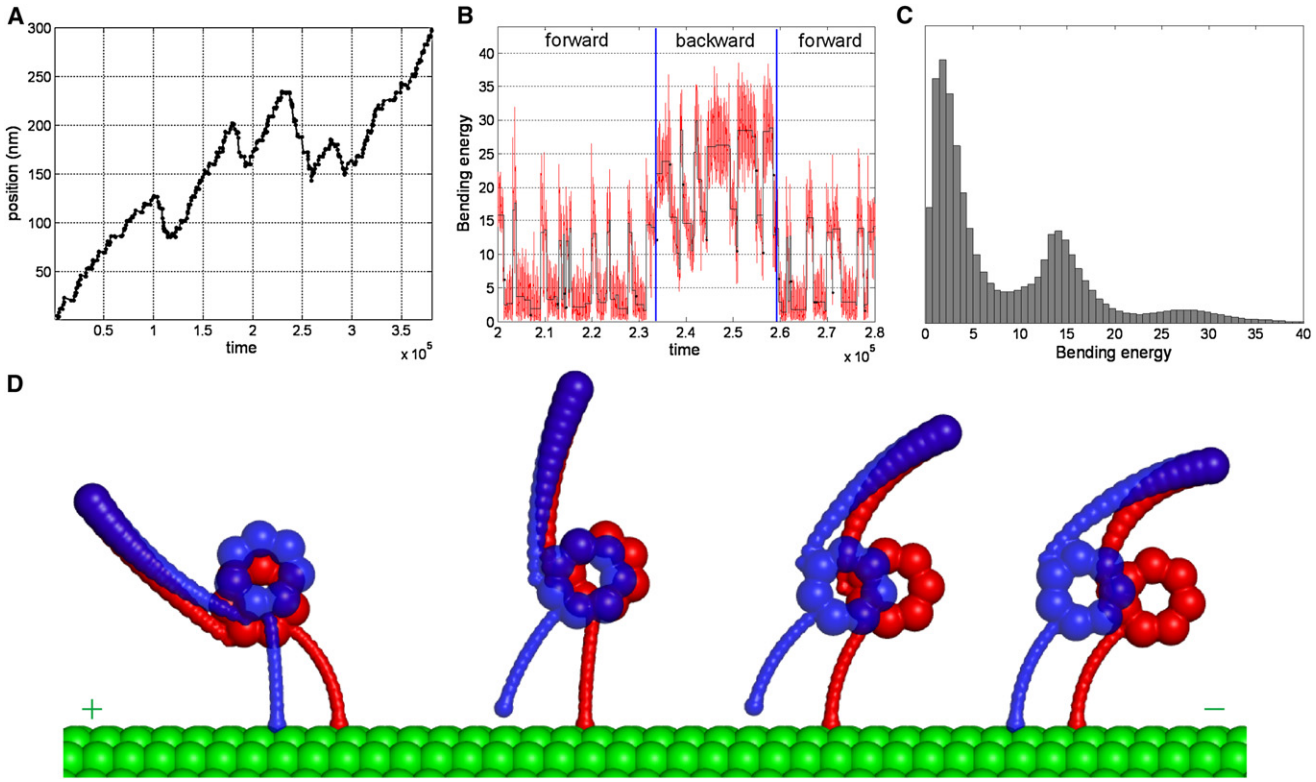

FIGURE 4 Simulations of processive motion. (*A*) Time series for dynein's movement along a microtubule. Stochastic transitions between the forward- and backward-stepping states are apparent. (*B*) Time series for the bending energy of the dimer (*thin trace*) corresponding to the time series shown in *A*. The thick trace shows the energy values averaged over the duration of the corresponding mechanochemical cycle. (*C*) Histogram of the bending energy from a long simulation showing three distinct maxima, corresponding to minima in bending energy. When the motor is trapped in the higher-energy states, it steps backward. In the lower-energy states, it moves forward. (*D*) A diagram demonstrating the transition from the low-energy forward-stepping state to the higher-energy state associated with backward stepping. After the free head transitions to the pre-power-stroke conformation, it binds to a site behind the bound head, which is in a post-power-stroke conformation. The motor is now poised for back-stepping (see also Fig. S4, Table S2, Movie S2, and Movie S3).

interaction is increased, the average time to reach a binding site grows, because the distribution for the free MTBD is no longer highly localized around the microtubule-binding site located 8.2 nm in front of the bound head (compare Fig. 2, *A* and *B*). Of interest, as the flexibility of the angle δ is further increased, the average search time decreases because binding sites behind and multiple sites in front of the attached head become accessible to the free head. Fig. 3 *D* shows that, in general, increased flexibility in the angle δ tends to decrease the velocity of the motor (defined here as the mean step size divided by the mean search time), because increased back-stepping outweighs the benefit of taking steps of $>$8.2 nm. However, more flexibility in the angle joining the tails can produce up to a 30% increase in the average velocity when the angle between the attached head and microtubule is sufficiently stiff (Fig. 3 *D*).

Full mechanochemical model of dimeric dynein

Finally, we combined our previously derived kinetic model for dynein's ATP hydrolysis cycle (11) with the structural model described above to produce a full mechanochemical model for homodimeric dynein. Computational simulations of the model involve a Monte Carlo method for biochemical transitions (ATP binding, ATP hydrolysis, and ADP and Pi release) and Langevin dynamics for mechanical transitions (power stroke, recovery, and attachment). Full details of the model are provided in the Supporting Material. Our previous kinetic analysis revealed that reproducing the experimentally measured velocity and processivity requires the assumptions that when the motor is in a compact conformation (i.e., both heads bound to the microtubule), ADP release from the rear head is increased and the front head's ability to complete the power stroke is impaired. We showed that including these state-dependent rates in our kinetic model tends to keep the ATP hydrolysis cycles of the two heads out of phase and allows the motor to achieve both high speed and high processivity. If mechanical strain from the attached rear head in the ADP state hinders the power stroke of the front head, it seems logical to assume that the power stroke of the front head would facilitate dissociation of the rear head. The dissociation rate of the rear head increases significantly once ATP binds to this head (10). A portion of this speed-up could indeed come from the power stroke, although our current model does not explicitly take this effect into account.

The behavior that results from the full model is presented in Fig. 4, *A–C*, and Movie S2. One unexpected property of the motor is the emergence of stochastic transitions between runs of processive forward and backward steps (Fig. 4 *A*). The backward-stepping state of the motor can be understood as follows: During a typical forward step, the attached head undergoes the power stroke and the free head transitions to the pre-power-stroke confirmation before reattaching to the site directly in front of the bound head. If instead the free head attaches to the microtubule site directly behind the bound head (Fig. 4 *D*, *rightmost conformation*), the motor is forced into a conformation that minimizes the bending energy (i.e., is stable) but is a higher-energy state than the global minimum assumed by the motor when the free head binds to the site in front of the bound head (Fig. 4 *D*, *leftmost conformation*). In this strained conformation, the leading head is more likely to detach and reattach to the site behind the bound head (backward stepping; Movie S3). However, thermal fluctuations eventually drive the motor back to the conformation that minimizes the bending energy, and the motor resumes forward stepping.

CONCLUSIONS

The existence of multiple local minima in the bending energy (Fig. 4, *B* and *C*) underlies the transitions between processive forward and backward stepping. This feature of dynein's motion was previously observed in experiments (20–23) in which the motor moved under external loads. In our model, the onset of successive back-steps does not require a force resisting forward motion. However, the assumptions used to simplify the model, or uncertainty in the flexibility of the angles δ and ξ, might underestimate the separation in bending energy of the local minima, making transitions to the strained state rare in the real motor without an applied force. In contrast to dynein, which exhibits runs of back-steps under substall forces, processive back-stepping in kinesin is observed only under superstall forces (24). Our model predicts that this difference is attributable to the existence of multiple equilibria in the dynein's bending energy, which presumably do not exist in the much smaller kinesin.

Although some evidence for cooperative interactions between dynein's two heads has been reported (13,25,26), a direct physical interaction between AAA^+ rings has not yet been demonstrated. Our model suggests a likely place for such an inter-ring interaction. During single forward steps, the simulations predict that the AAA^+ rings of the two heads maintain a compact conformation (i.e., remain in close proximity). Surprisingly, there is a point on the two ring domains that tends to undergo purely horizontal motion throughout the step cycle (Movie S1), i.e., it acts as pivot about which the heads rotate in opposite directions. The point is located between the fifth and sixth AAA domains of the ring (5.60 nm from the ring center and 53.7° from the point where the stalk emerges). An interhead interaction at this point (electrostatic or hydrophobic) with rotational freedom would not interfere with the heads' motion during forward steps of 8.2 nm, but would prevent longer steps and back-stepping from occurring. Therefore, our model predicts this site as a likely point for the two heads to interact. Of interest, this site is located in the region where EM mapping predicts the location of the head's C-sequence domain (16). Numata et al. (27) examined the role of the C-sequence in dynein's motility. The authors concluded that the distal C-sequence segment may affect the motor's processivity by interfering with an interhead interaction. Our results are consistent with this conclusion.

The most important feature of dynein's mechanochemical cycle revealed by our simulations is that the motor's structure causes the MTBD of the free head to remain in close proximity to the microtubule as the MTBD moves toward the next binding site (Fig. S3 *A*, Movie S1, and Movie S2). That is, the motion of the MTBD is essentially constrained to one dimension. This reduction of dimension greatly improves the efficiency with which the free head finds the appropriate binding site.

We also find that the power stroke by itself is not sufficient to move the free head from a binding site behind the attached head to one in front. Reaching the forward site also requires the free head to recover from the post- to pre-power-stroke conformation. That is, recovery is not simply a passive process required to reset the motor domain; it is an integral part of dynein's step cycle that allows the motor to move efficiently in the forward direction (Fig. 1 *E*).

In summary, we have developed a full mechanochemical model for the motor protein dynein. The model is consistent with the known biochemical and biophysical properties of the motor and provides a detailed explanation for how this large and complex molecule efficiently moves unidirectionally along microtubules. Our hope is that the results presented here will inspire new experimental designs to test the predictions of the model.

APPENDIX

Our model is built from structural data extracted from EM images that resolve conformational changes of dynein's motor domains in the plane of the AAA^+ ring (14). Other experimental results demonstrate that dynein's motion is primarily in a plane parallel to the axis of the microtubule (6,28). Thus, if we ignore occasional side-stepping, our two-dimensional model should faithfully represent the motor's dynamics.

The geometry of the AAA^+ ring is taken to be a circle of radius R. The stalk and tail are assumed to be flexible but inextensible, with lengths L_s and L_t, respectively. The stalk is assumed to emerge perpendicularly from the AAA^+ ring (17), whereas the tail emerges tangentially. The line segments from the center of the AAA^+ ring to the points of emergence of the stalk and the tail define the angle γ. These considerations allow the conformation of each head to be described by the following set of variables: $\{\alpha = L_s/R_s,\ \beta = L_t/R_t,\ \gamma\}$, where R_s and R_t are the radius of curvature for the stalk and the tail, respectively (Fig. 1 *D*, Fig. S1 *A*, and Fig. S2 *A*).

The distributions for the variables α, β, and γ are different in the pre- and post-power-stroke conformations, with the most pronounced difference being the mean values of γ. To simulate transitions between the pre- and

post-power-stroke conformations, we introduce a double-well potential, E_γ, with local minima at $(\gamma_{post} = 28.5^\circ, E_{post})$ and $(\gamma_{pre} = 86.0^\circ, E_{pre})$ (Fig. S4, *A* and *B*). Mathematically, this potential is described by three smoothly connected parabolas, so that the pre- and post-power-stroke conformations correspond to $E_{pre}<E_{post}$ and $E_{pre}>E_{post}$, respectively (Fig. S4, *A* and *B*). Stochastic switching between the two potentials simulates the power stroke and recovery, and corresponds to an overall free-energy change of $2\ |E_{pre} - E_{post}|$, which is set equal to the free energy available from the ATP hydrolysis (29).

The mean diffusion velocity (Fig. 3 *D*) is calculated using the expression $\langle v\rangle = \sum_i (s_i \cdot f_i)/\langle\tau\rangle$, where s_i is the discrete step size, f_i is the normalized frequency of occurrence of the step size s_i (Fig. 3 *A*), and $\langle\tau\rangle$ is the mean time for the free head to bind the microtubule (Fig. 3 *C*).

Further details on incorporating simulations of dynein's structural dynamics into Monte Carlo simulations of the motor's ATP hydrolysis cycle (11) (Fig. S4 *C*) are provided in the Supporting Material.

SUPPORTING MATERIAL

Additional text, references, four figures, a table, and three movies are available at http://www.biophysj.org/biophysj/supplemental/S0006-3495(11)00613-8.

We thank Michael E. Fisher (Institute for Physical Science and Technology, University of Maryland) for his comments and constructive criticism of the manuscript.

This work was supported by the National Institutes of Health (grants R01HL077546-03 and R01GM079271 to T.E., and grant R01GM080742 and American Recovery and Reinvestment Act supplement GM080742-03S1 to N.D.).

REFERENCES

1. Vallee, R. B., J. C. Williams, …, L. E. Barnhart. 2004. Dynein: an ancient motor protein involved in multiple modes of transport. *J. Neurobiol.* 58:189–200.
2. Koonce, M. P., and M. Samsó. 2004. Of rings and levers: the dynein motor comes of age. *Trends Cell Biol.* 14:612–619.
3. Vale, R. D. 2003. The molecular motor toolbox for intracellular transport. *Cell.* 112:467–480.
4. Wade, R. H. 2009. On and around microtubules: an overview. *Mol. Biotechnol.* 43:177–191.
5. Holzbaur, E. L., and R. B. Vallee. 1994. DYNEINS: molecular structure and cellular function. *Annu. Rev. Cell Biol.* 10:339–372.
6. Mizuno, N., A. Narita, …, M. Kikkawa. 2007. Three-dimensional structure of cytoplasmic dynein bound to microtubules. *Proc. Natl. Acad. Sci. USA.* 104:20832–20837.
7. Carter, A. P., J. E. Garbarino, …, I. R. Gibbons. 2008. Structure and functional role of dynein's microtubule-binding domain. *Science.* 322:1691–1695.
8. Ueno, H., T. Yasunaga, …, K. Hirose. 2008. Dynein pulls microtubules without rotating its stalk. *Proc. Natl. Acad. Sci. USA.* 105:19702–19707.
9. Mogami, T., T. Kon, …, K. Sutoh. 2007. Kinetic characterization of tail swing steps in the ATPase cycle of *Dictyostelium* cytoplasmic dynein. *J. Biol. Chem.* 282:21639–21644.
10. Imamula, K., T. Kon, …, K. Sutoh. 2007. The coordination of cyclic microtubule association/dissociation and tail swing of cytoplasmic dynein. *Proc. Natl. Acad. Sci. USA.* 104:16134–16139.
11. Tsygankov, D., A. W. Serohijos, …, T. C. Elston. 2009. Kinetic models for the coordinated stepping of cytoplasmic dynein. *J. Chem. Phys.* 130:025101.
12. Higuchi, H., and S. A. Endow. 2002. Directionality and processivity of molecular motors. *Curr. Opin. Cell Biol.* 14:50–57.
13. Shima, T., K. Imamula, …, K. Sutoh. 2006. Head-head coordination is required for the processive motion of cytoplasmic dynein, an AAA^+ molecular motor. *J. Struct. Biol.* 156:182–189.
14. Burgess, S. A., M. L. Walker, …, K. Oiwa. 2003. Dynein structure and power stroke. *Nature.* 421:715–718.
15. Serohijos, A. W., D. Tsygankov, …, N. V. Dokholyan. 2009. Multiscale approaches for studying energy transduction in dynein. *Phys. Chem. Chem. Phys.* 11:4840–4850.
16. Roberts, A. J., N. Numata, …, S. A. Burgess. 2009. AAA^+ Ring and linker swing mechanism in the dynein motor. *Cell.* 136:485–495.
17. Carter, A. P., C. Cho, …, R. D. Vale. 2011. Crystal structure of the dynein motor domain. *Science.* 331:1159–1165.
18. Reck-Peterson, S. L., A. Yildiz, …, R. D. Vale. 2006. Single-molecule analysis of dynein processivity and stepping behavior. *Cell.* 126: 335–348.
19. Toba, S., T. M. Watanabe, …, H. Higuchi. 2006. Overlapping hand-over-hand mechanism of single molecular motility of cytoplasmic dynein. *Proc. Natl. Acad. Sci. USA.* 103:5741–5745.
20. Shingyoji, C., H. Higuchi, …, T. Yanagida. 1998. Dynein arms are oscillating force generators. *Nature.* 393:711–714.
21. Gennerich, A., A. P. Carter, …, R. D. Vale. 2007. Force-induced bidirectional stepping of cytoplasmic dynein. *Cell.* 131:952–965.
22. Bullock, S. L., A. Nicol, …, D. Zicha. 2006. Guidance of bidirectional motor complexes by mRNA cargoes through control of dynein number and activity. *Curr. Biol.* 16:1447–1452.
23. Ross, J. L., K. Wallace, …, E. L. Holzbaur. 2006. Processive bidirectional motion of dynein-dynactin complexes in vitro. *Nat. Cell Biol.* 8:562–570.
24. Carter, N. J., and R. A. Cross. 2005. Mechanics of the kinesin step. *Nature.* 435:308–312.
25. Iyadurai, S. J., M. G. Li, …, T. S. Hays. 1999. Evidence for cooperative interactions between the two motor domains of cytoplasmic dynein. *Curr. Biol.* 9:771–774.
26. Ori-McKenney, K. M., J. Xu, …, R. B. Vallee. 2010. A cytoplasmic dynein tail mutation impairs motor processivity. *Nat. Cell Biol.* 12:1228–1234.
27. Numata, N., T. Shima, …, K. Sutoh. 2011. C-sequence of the *Dictyostelium* cytoplasmic dynein participates in processivity modulation. *FEBS Lett.* 585:1185–1190.
28. Oda, T., N. Hirokawa, and M. Kikkawa. 2007. Three-dimensional structures of the flagellar dynein-microtubule complex by cryoelectron microscopy. *J. Cell Biol.* 177:243–252.
29. Mogilner, A., H. Wang, T. Elston, and G. Oster. 2002. Molecular motors: theory. *In* Computational Cell Biology. C. P. Fall, E. S. Marland, J. M. Wagner, and J. J. Tyson, editors. Springer, New York. 321–355.